Editors' Suggestion

From hindered to promoted settling in dispersions of attractive colloids: Simulation, modeling, and application to macromolecular characterization

Andrew M. Fiore, Gang Wang, and James W. Swan*
Department of Chemical Engineering, Massachusetts Institute of Technology, Cambridge, Massachusetts 02139, USA

(Received 28 March 2018; published 15 June 2018)

The settling of colloidal particles with short-ranged attractions is investigated via highly resolved immersed boundary simulations. At modest volume fractions, we show that intercolloid attractions lead to clustering that reduces the hinderance to settling imposed by fluid back flow. For sufficient attraction strength, increasing the particle concentration grows the particle clusters, which further increases the mean settling rate in a physical mode termed *promoted* settling. The immersed boundary simulations are compared to recent experimental measurements of the settling rate in nanoparticle dispersions for which particles are driven to aggregate by short-ranged depletion attractions. The simulations are able to quantitatively reproduce the experimental results. We show that a simple, empirical model for the settling rate of adhesive hard-sphere dispersions can be derived from a combination of the experimental and computational data as well as analytical results valid in certain asymptotic limits of the concentration and attraction strength. This model naturally extends the Richardson-Zaki formalism used to describe hindered settling of hard, repulsive spheres. Experimental measurements of the collective diffusion coefficient in concentrated solutions of globular proteins are used to illustrate inference of effective interaction parameters for sticky, globular macromolecules using this empirical model. Finally, application of the simulation methods and empirical model to other colloidal systems are discussed.

DOI: 10.1103/PhysRevFluids.3.063302

I. INTRODUCTION

Settling of dispersed colloidal particles is central to the processing and analysis of a wide range of industrial and scientific materials. Centrifugation is used as both a processing and analytical tool in laboratory and commercial settings [1], and gravity-driven particle motion controls the shelf life of many consumer and food products [2]. In the context of environmental science, sedimentation of suspended particles plays a crucial role in the engineering of pollution remediation strategies [3] as well as natural processes of erosion and deposition [4]. Additionally, there is a linear relationship between the sedimentation coefficient and the collective diffusivity in colloidal dispersions. Thus, important industrial separation processes such as ultrafiltration applied to purification of biologically derived macromolecules, whose design requires accurate models of the collective diffusivity, depend on knowledge of the sedimentation coefficient in concentrated dispersions [5]. In a vast majority of these materials and systems, the colloidal particles are attractive. However, most fundamental studies of settling in colloidal dispersions concern hard or repulsive particles. In the present work, we apply the immersed boundary method to study the settling rate in concentrated dispersions of spherical colloids with short-ranged attractions.

*jswan@mit.edu

The settling dynamics of concentrated colloidal dispersions are controlled by the hydrodynamic interactions induced as moving particles displace the surrounding fluid. The flows generated by settling particles decay to leading order as the inverse of the distance from the particle. The entrainment of other particles by these disturbance flows is a critical factor in settling dispersions. The combined flow produced by all the settling particles appears to diverge with the physical size (extent) of the dispersion because of the long-ranged nature of these hydrodynamic interactions [6]. However, mass conservation at the system boundaries produces a backflow driven by a pressure gradient balancing the buoyant weight of the particles. When the backflow is combined with the induced flows, an intensive sedimentation rate, one that is independent of the system size, results. The interplay of entrainment and backflow is a subtle one that makes the sedimentation a sensitive function of the microstructure of the colloidal dispersion. In dispersions of attractive colloids, which tend to form clusters, entrainment and backflow act synergistically so that attractions always accelerate the settling process. The reasons for this are straightforward: Clusters in isolation naturally sediment more quickly than individual particles, and the widened spaces between clustering particles lead to a weaker resistance due to the backflow. Quantifying these effects represents a major challenge in quantitative colloid science. In the present work, we consider a limit in which the Péclet number for the settling particles is vanishingly small. In this limit, the rate of particle diffusion far exceeds the rate of sedimentation and the microstructure of the colloidal dispersion is dictated by thermodynamic equilibrium.

Of the limited studies on the sedimentation of attractive suspensions, the most important result, a dilute-limit approximation for the mean settling rate U of a suspension of spherical particles, accurate to first order in the particle volume fraction ϕ, was derived by Batchelor more than 50 years ago [7,8]:

$$\frac{U}{U_0} = 1 - 6.55\,\phi + 3.52\,(1 - B_2^*)\,\phi + \mathcal{O}(\phi^2), \tag{1}$$

where U_0 is the settling speed of a single isolated particle and $B_2^* = B_2/B_2^{HS}$, where B_2 is the second virial coefficient of the particles and B_2^{HS} is the second virial coefficient of a reference hard-sphere dispersion. For dilute hard spheres, entrainment and backflow combine to reduce the relative settling rate of particles by an amount of $6.55\,\phi$. Attractive interactions cause B_2^* to drop from unity (hard spheres) to negative values. This has the effect of increasing the settling speed relative to hard spheres. For sufficiently strong attractions ($B_2^* \leqslant -0.861$), Batchelor's theory predicts that a dispersion can settle faster than an isolated particle. Moncho-Jordá *et al.* used a series of stochastic rotation dynamics (SRD) simulations to test Batchelor's dilute limit prediction as well as to study sedimentation in concentrated attractive dispersions. They observed that particles with attractive interactions sediment more quickly than hard spheres at all volume fractions and that, within a specific range of volume fractions, sufficiently strong attractions produce a settling rate that is larger than even the isolated particle value. For dispersions that exhibited such promoted settling, the sedimentation rate exhibited a nonmonotonic dependence on particle volume fraction. At low volume fractions, the rate increases above the single-particle value. Beyond a critical volume fraction, the settling rate decreased as expected of conventional hindered settling. These simulations and the resulting data possess a number of physical and quantitative issues, including being performed at finite but small Péclet and Reynolds numbers, being limited in the number of particles represented in the periodic simulation box, and having made no systematic finite-system-size corrections to the measured sedimentation rates. Inspired by these simulations, Lattuada *et al.* conducted an experimental study designed to corroborate the simulation results [9]. They found a qualitative agreement between the experiments and simulations. However, they observed that the SRD simulations systematically underpredict the settling rate of attractive suspensions measured experimentally and also underpredict the range of volume fractions over which promoted settling is observed. These studies are the first steps toward understanding the settling of concentrated solutions of attractive particles, but much remains unexplored. For example, a predictive microstructural model for the settling rate would be very useful in applications involving attractive colloidal dispersions.

In the present work, we use immersed boundary simulations in the limits of zero Péclet and Reynolds numbers to systematically investigate the effect of attraction strength and particle volume fraction on the mean settling rate. We show that these simulations, which account properly for finite-system-size effects, reproduce experimental measurements quantitatively. Furthermore, we develop an empirical model for the settling rate based on a measure of microstructure in attractive dispersions that quantitatively matches experimental data and our own simulation data at all the volume fractions studied.

II. SIMULATION METHODOLOGIES

We compute the settling rate of attractive colloidal dispersions using an immersed boundary method referred to colloquially as the composite bead [10] or rigid multiblob [11] approach. The details of the computational method are described elsewhere [10]. Here we give a brief review. In this approach, the surface of each colloidal particle is approximated by a collection of beads that interact hydrodynamically. Each bead generates a regularized Stokeslet flow and is entrained by flows induced by other particles in a reciprocal fashion [12,13]. In our formulation, the Rotne-Prager-Yamakawa tensor [14] that linearly relates the force exerted on one bead to the entrained velocity of another bead is used to represent these flows. Additionally, the beads tessellating the surface of each particle are constrained to move as a rigid body. A set of Lagrange multipliers, forces that ensure the constraints are satisfied, are introduced and a system of linear equations is solved to determine the rigid-body motions of the colloidal particles and the Lagrange multipliers in response to any set of imposed external forces. In the present work, the spectral Ewald method [15] is used to evaluate the product of the Rotne-Prager-Yamakawa (RPY) tensor for all the beads with an arbitrary set of forces acting on the beads. The linear equations governing the rigid-body motions and the Lagrange multipliers are solved using the generalized minimum residuals (GMRES) methodology with constraint preconditioning [16]. In summary, this approach can be used to evaluate the transport properties of macromolecular and colloidal solutions of arbitrarily shaped particles in $O(N)$ time, where N is the total number of beads used to discretize the surface of all the colloids. Importantly, this model correctly captures the effect of fluid backflow on the sedimentation velocity. Because of fluid incompressibility, the downward volume flux of sedimenting particles is exactly balanced by an upward volume flux of fluid, termed backflow. In the RPY model, the fluid incompressibility is exactly enforced by setting the zero-wave-vector component of the fluid velocity to be zero. Mathematically, the fluid backflow originates from the particle quadrupole, which is implicit in our model through the rigid-body constraint, which forces the fluid contained within a composite bead particle to move as a rigid body and therefore displace an equal volume of fluid as it sediments.

For the spherical colloids studied here, the beads are made to sit on the vertices of an icosphere formed by subdividing the faces of a Goldberg polyhedron (see Fig. 1). We have shown how such a discretization can be used to replicate the hydrodynamic interactions among a pair of spherical particles in a previous publication [10]. Convergence of the calculation with respect to the number of beads is slow for relative motion between particles because of the effects of hydrodynamic lubrication. However, convergence is fast for collective modes of motion. Figure 1 also depicts the convergence of the sedimentation rate of a cubic array of spherical colloids as a function of the number of beads tessellating the surface. Zick and Homsy performed high-accuracy calculations of lattice sedimentation and published their results with three digits of accuracy [17]. We find that 2562 beads per colloid is sufficient to exactly reproduce the published results, and therefore use the solution with 2562 as the reference state for the convergence study. With just 162 beads per colloid, the classic results of Zick and Homsy are recovered to within 5% for the full range of volume fractions studied. Therefore, in the present calculations we use 162 beads per colloid. This level of discretization is chosen to accommodate a balance between the number of colloids required to accurately model the microstructure of an attractive dispersion, the number of realizations of that microstructure needed to compute statistically meaningful averages, and the total computation time of the simulation. It is known that number density fluctuations are large in attractive colloidal dispersions. Additionally, the

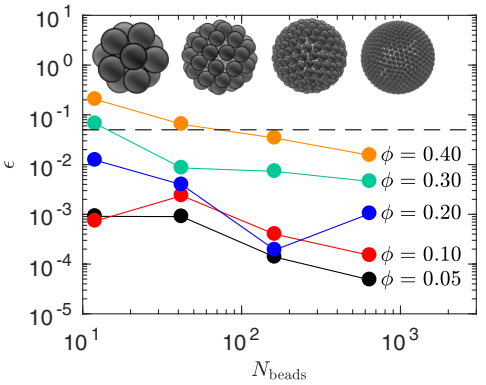

FIG. 1. Relative error in the mean sedimentation rate of a periodic simple cubic lattice of spherical particles computed using the icosphere approximation of the spherical surface compared to a high-resolution approximation ($N_{\text{bead}} = 2562$) as a function of the number of vertices of the polyhedron, N_{bead}, at different volume fractions, ϕ. We find that $N_{\text{bead}} = 2562$ is sufficient to exactly reproduce the published data of Zick and Homsy [17]. The polyhedra used in the calculations are shown above the associated points. The black dashed line denotes 5% relative error.

magnitude of velocity fluctuations among sedimenting colloids can be of the same order of magnitude as the mean sedimentation velocity [18]. Thus, 1000 colloids are modeled and averages of the settling velocity are constructed from 1000 independent snapshots of the dispersion microstructure. Throughout this work, fluctuations in the settling rate among different configurations are used to quantify a standard error at the 95% confidence level.

The experiments of Lattuada *et al.* control interparticle attraction by adding surfactant micelles to solution in order to induce depletion [9]. Therefore, we model the interaction potential, $V(r)$, with a short-ranged attraction described by the Asakura-Oosawa depletion potential [19] plus a hard-core repulsion at interparticle contact, $r = 2a$:

$$V(r) = \begin{cases} \infty & r < 2a \\ -\varepsilon \frac{(a+\delta)^3}{\delta^2 (1.5a+\delta)} \left[1 - \frac{3}{4}\frac{r}{a+\delta} + \frac{1}{16}\left(\frac{r}{a+\delta}\right)^3\right] & r \geqslant 2a \end{cases}, \tag{2}$$

where ε is the strength of the attraction at contact and δ is the range of the attraction. The Asakura-Oosawa potential was validated in these experiments through measurements of the osmotic compressibility in the colloidal dispersion. The range of the depletion potential is chosen to match the experiments: $\delta/a = 0.028$. The depletion potential at contact, ε, is varied and can be chosen so that simulated dispersions match the experimentally measured second virial coefficient, B_2^*. Consistent with experiments, 5% dispersity in particle size is introduced to suppress crystallization in the simulations.

The experimental value of the Péclet number is small, $\text{Pe} = 4\pi\Delta\rho g a^4/3k_BT \approx 10^{-3}$, where $\Delta\rho$ is the density difference between the immersed colloids and the fluid, g is the gravitational constant, and k_B is Boltzmann's constant, so the distribution of particle positions during settling is very close to the equilibrium distribution. Therefore, simple, freely draining Brownian dynamics simulations of single beads are used to generate representative configurations of the particles from which the mean settling rate can be computed. For each combination of ϕ and ε (or B_2^*), an initial hard-sphere configuration of spherical colloids is allowed to relax for 1000 bare diffusion times ($6\pi\eta a^3/k_BT$). Then, snapshots of the particle configuration are taken every 10 bare diffusion times until 1000 snapshots have been accumulated. For each snapshot, a composite-bead representation of all the particles is constructed from 162 bead icospheres having randomly assigned orientations. The mean settling rate for each configuration is determined by applying a uniform force to each

bead and computing the mean of the resulting rigid-body translational velocities of the colloids. The computed mean velocity is sensitive to the periodic boundary conditions in the simulations, and the infinite system size limit U^∞ is found by

$$U^\infty = U + 1.7601\, S(0) \left(\frac{\eta_s}{\eta(\phi)}\right) \left(\frac{\phi}{N}\right)^{1/3}, \tag{3}$$

which is the finite-size correction given by Ladd *et al.* [20], where $S(0)$ is the value of the static structure factor at zero wave number, η_s is the solvent viscosity, and $\eta(\phi)$ is the high-frequency viscosity, which we compute for each configuration. It should be noted that although we use the depletion potential to model the particle attractions, with this procedure any sufficiently short-ranged potential will produce equivalent equilibrium structures [21]. The Noro-Frenkel rule of corresponding states suggests that samples of these equilibrium structures can be drawn from a mapping onto the Baxter adhesive hard-sphere interaction potential. In Sec. III B, we discuss this mapping explicitly. Therefore, the results presented in this paper should be generic for any colloidal dispersion aggregating due to short-ranged attractions.

III. RESULTS AND DISCUSSION

A. Comparison of simulations and experiments

There is limited experimental data available for the mean settling rate of colloids as a function of concentration for different well-characterized attraction strengths. Lattuada *et al.* provide data at three different attraction strengths, characterized by the reduced second virial coefficients: $B_2^* = 1.0, -0.27, -1.08$ [9]. These values correspond to hard-sphere interactions (no attraction), a modest attraction ($\varepsilon = 4.84\, k_B T$), and a strong attraction ($\varepsilon = 5.18\, k_B T$) that is near the boundary for liquid-liquid phase separation, respectively. The experiments were performed with particle volume fractions, ϕ, as large as $\phi = 0.20$. We compute the mean settling rate for each of the experimental values of B_2^* for $0.01 \leqslant \phi \leqslant 0.40$. Figure 2 shows our simulation results, the experimental data of Lattuada *et al.*, and the simulation data of Moncho-Jordá *et al.* Our results are in quantitative agreement with the experimental data for all values of B_2^* and ϕ for which a comparison is available. The SRD simulation results of Moncho-Jordá *et al.* display only qualitative agreement with our simulations and the experimental data, and predict a much sharper decay of U with ϕ than is observed experimentally for the two attractive dispersions studied. The agreement between experiments and our simulations

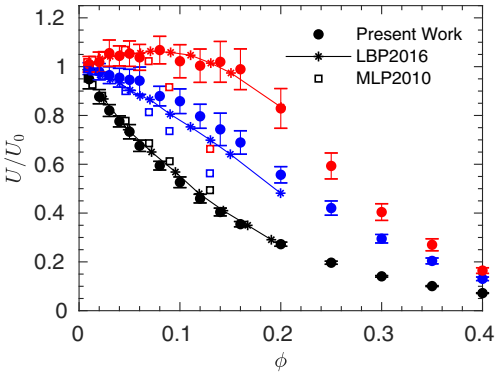

FIG. 2. Normalized settling velocity as a function of particle volume fraction for $B_2^* = -1.08$ (red), $B_2^* = -0.27$ (blue), and $B_2^* = 1$ (black) from the experimental data of Ref. [9] (stars with lines, denoted LBP2016 in the legend) and computed in the present work (filled circles) and the SRD simulations of Ref. [22] as interpolated in Ref. [9] (open squares, denoted MLP2010 in the legend). Error bars represent the standard error of the observed measurements.

affirms our claim that the proposed simulation methodology is appropriate to perform a systematic study the sedimentation rate as a function of particle volume fraction and attraction strength.

It is a challenge to assess the discrepancy between the SRD simulations and our own. A number of factors may be at play. One central problem is a failure of Moncho-Jordá *et al.* to account for finite-system-size effects in the calculation of the settling rate. As in Eq. (3), in periodic geometries transport properties like settling rate and diffusivity are depressed by an amount proportional to $aV^{-1/3}$, where V is the volume of the simulation cell. For simulations with a fixed number of particles, increasing the volume fraction acts to decrease V, which further depresses the computed values of transport properties. However, to change volume fraction, Moncho-Jordá *et al.* fix the simulation volume and increase N. So a systematic depression of the settling rate due to finite-system-size effects alone is not enough to explain their data. A further issue that may explain the discrepancy with their simulations is the finite Péclet number used in that study. The authors estimate that $\mathrm{Pe} \approx 2.5$ in their *dynamic* simulations, which means that deviations from equilibrium distribution for the particle configuration are inevitable. The effect of Pe on the mean settling rate of dispersions is also not well studied. However, for hard spheres in the dilute limit and at large Peclet numbers, Cichocki and Sadlej [23] have shown that a different expression for the sedimentation rate is expected: $U/U_0 = 1 - 3.87\phi$. The settling rate is a sensitive function of the structure, and the settling process modeled dynamically by the SRD simulations may have exhibited changes from the equilibrium structure and even structural anisotropy promoted by the hydrodynamic interactions among the particles. In the present study, the Peclet number is set asymptotically to zero and only the equilibrium structure is used for the calculation of the transport properties.

B. Microstructural characterization and corresponding states

As is common for colloids with short-ranged attractions, Lattuada *et al.* characterized the attraction strength in their dispersion using the Baxter temperature, τ. The Baxter temperature is a parameter that arises in the adhesive hard-sphere (AHS) model of attractive particles, in which the interparticle potential has vanishing width and infinite depth, but is characterized by a single parameter, τ, reflecting the propensity of particles to adhere to one another [24]. This parameter is a measure of the effective strength of attraction in the suspension, with smaller values corresponding to stronger attractions. B_2^* for the AHS model can be related to the Baxtern temperature, τ, as $B_{2,\mathrm{AHS}}^* = 1 - 1/(4\tau)$. In the approach taken by Lattuada *et al.*, τ is computed by matching the measured B_2^* to the analytical expression for B_2^* of AHS model, so that

$$\tau = \tfrac{1}{4}(1 - B_2^*)^{-1}. \tag{4}$$

Assigning a value to τ in this fashion provides a way of determining the dilute limit thermodynamic and transport properties of dispersions with short-ranged attractions in a fashion that is agnostic to the details of the interaction potential. However, values of τ computed by (4) are valid only in the dilute limit. As the dispersion concentration increases, τ changes even for fixed B_2^*, and as a result more detailed models are required to infer τ for dispersions of arbitrary concentration.

In the original development of the AHS model, Baxter produced an analytical expression for the Percus-Yevick (PY) approximation to the pair distribution function $g(r)$ of sticky particles [24,25]. The AHS model results in an expression for $g(r)$ that is completely parameterized by the particle size a, ϕ, and the effective "stickiness" parameter—the Baxter temperature—τ. An analytical expression for the static structure factor, $S(q)$, of an AHS suspension can be directly computed from Baxter's result [26]. Applying the Noro-Frenkel rule of corresponding states, which states that the thermodynamic properties, including dispersion microstructure, of colloids with short-ranged attractions can all be mapped back onto the adhesive hard-sphere model, the stickiness parameter, τ, for a concentrated dispersion of colloids with short-range attractions can be inferred from calculations of either $g(r)$ or $S(q)$ (or any other state function) for that dispersion. For any of these functions, the calculated values can be fit by analytical expressions from the adhesive hard-sphere model at the same particle concentration to determine a corresponding value for τ. In the dilute limit, using the

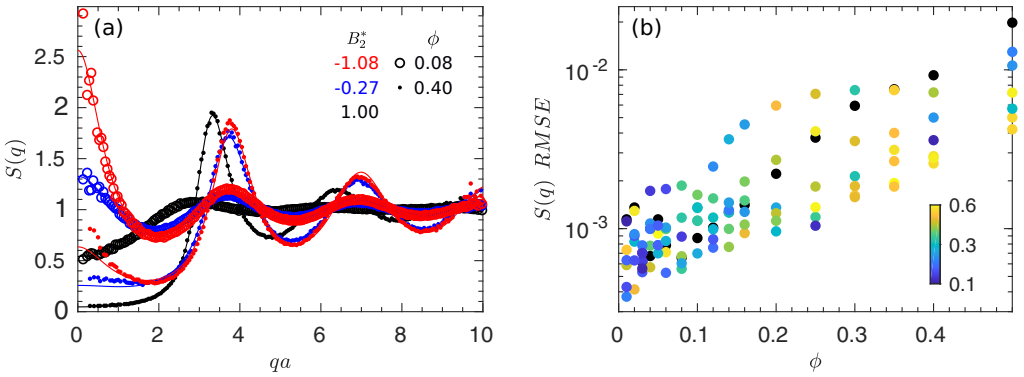

FIG. 3. (a) Static structure factor computed for the three attraction strengths reported in Fig. 2, $B_2^* = -1.08$ (red), $B_2^* = -0.27$ (blue), and $B_2^* = 1$ (black), at $\phi = 0.08$ (open circles) and $\phi = 0.40$ (dots). The lines are fits by the AHS solution to the Percus-Yevick approximation for $S(q)$. The τ values computed for the fit are 10.53, 0.16, and 0.11 for the black, blue, and red data sets, respectively at $\phi = 0.08$ and 6.53, 0.21, 0.12 for the respective data sets at $\phi = 0.40$. (b) Root-mean-squared error of the AHS Percus-Yevick solution to the simulation data colored by the inferred τ value, with black corresponding to hard spheres.

osmotic pressure as the state function will recover (4). For more concentrated dispersions, $S(q)$ [or $g(r)$] is required to determine the particular value of τ that characterizes the thermodynamic state of the dispersion in the corresponding adhesive hard-sphere model. For this reason, throughout this paper τ is an *a priori* unspecified parameter which is inferred from simulation data.

Figure 3 shows the values of $S(q)$ computed at the three attraction strengths from Fig. 3 at $\phi = 0.08$ and $\phi = 0.40$, compared to the PY approximation for adhesive hard spheres using a value of τ inferred by minimizing the root-mean-squared error (RMSE) of the PY model with respect to the computed data. Excellent agreement is observed between the model and the data for the six examples shown. Similar agreement of the PY model with the fit structure factor is associated with other particle concentrations and attraction strengths. Figure 3(b) shows the relative error in the computed static structure factor with respect to the Percus-Yevick approximation at the best-fit value of τ as a function of the colloid volume fraction and the second virial coefficient for all the simulated dispersions. Errors smaller than 1% are typical, indicating that the fitting procedure is adequate for characterizing the suspension microstructure in terms of the generalized stickiness parameter. This fitting procedure can be generalized to experimental data with sticky macromolecules of known number density, n, as discussed in Sec. III D. In this way, measurements of $S(q)$, allows mapping onto the AHS model without *a priori* knowledge of either B_2^*. The pair τ and the volume fraction serve as unique descriptors of the attractive suspension microstructure and as we will show the value of this pair also fixes the mean settling rate.

C. Settling rate as a function of ϕ and τ

We performed simulations systematically varying B_2^* between -1.48 and 1.00 and ϕ from 0.01 to 0.50 for a dispersion of spherical colloids interacting via a depletion potential with $\delta/a = 0.028$. Each set of parameters is characterized by the τ value inferred from $S(q)$. Shown in Fig. 4(a) is the mean settling rate as a function of volume fraction and inferred Baxter temperature normalized by the single particle value, U/U_0, where the color of the symbols corresponds to the inferred value of τ, with the results for hard spheres are depicted in black.

At a fixed concentration, as τ increases, the settling velocity decreases and approaches the hard-sphere limit, $\tau \to \infty$. Furthermore, although the shape of U/U_0 is strongly dependent on τ at low ϕ, at sufficiently large ϕ, the settling velocity exhibits a qualitative similarity for all τ. With increasing concentration, the influence of the stickiness parameter on the settling rate is diminished. In this

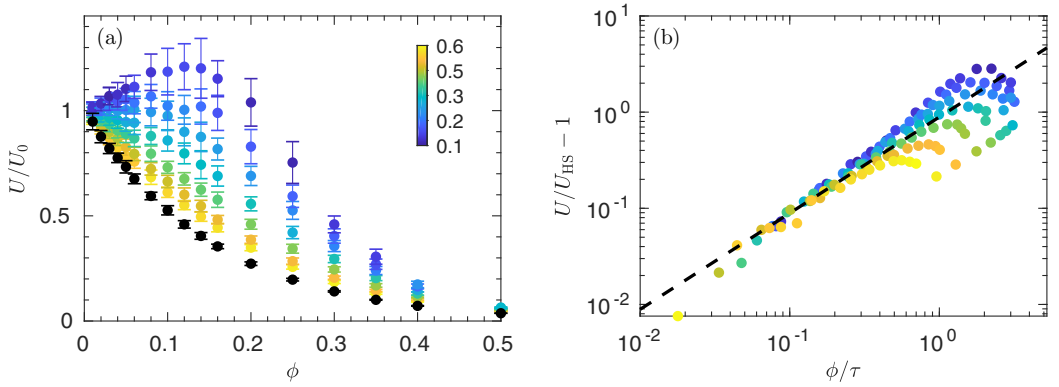

FIG. 4. (a) Normalized settling velocity as a function of particle volume fraction for $-1.48 \leqslant B_2^* \leqslant 1.00$ colored by the value of the stickiness parameter τ inferred from the static structure factor (black is hard-sphere data). (b) Relative difference between the settling rate of attractive and hard-sphere dispersions for each condition presented in panel (a). The dashed black line denotes the Batchelor result in the limit $\phi \to 0$: $0.89\phi/\tau$.

regime, particles fill space rather homogeneously, regardless of τ, and the sedimentation rate decays to zero much as with hard spheres. Attractions between particles still increase the sedimentation rate slightly by introducing small heterogeneities in the microstructure that are indicated by an increase in the value of $S(q)$ as $q \to 0$. These void spaces allow backflow to occur with less resistance, thus slightly increasing the settling rate.

The simulation data show a transition in the shape of the settling curves as both τ and ϕ are increased. For hard spheres, U/U_0 is monotonically decreasing and concave up for all ϕ. At modest attractions, U/U_0 is still monotonically decreasing but is initially concave down until an inflection point around $\phi = 0.2$. An inflection point is also observed for strong attractions, $\tau \lesssim 0.2$, but U/U_0 is no longer monotonic. The settling rate increases until $\phi \approx 0.10$, where it exhibits a maximum rate of promoted settling. Then, the settling rate decays much as for hard spheres.

The ratio of the sedimentation rate of attractive particle dispersions to a hard-sphere dispersion at the same concentration is shown in Fig. 4(b) as a function of ϕ/τ. ϕ/τ is the natural parameter that appearing in Batchelor's dilute-limit result, when substituting the second virial coefficient with the AHS model [8]. Batchelor's model describes the ratio well for for $\phi/\tau \lesssim 0.5$. For $\phi/\tau \gtrsim 0.5$, the data are no longer a function of ϕ/τ alone and exhibit a sharp downturn with increasing ϕ/τ.

To develop an empirical model for sedimentation in attractive dispersions at arbitrary volume fractions, we start with the Richardson-Zaki correlation [27], which is a common model for settling in suspensions,

$$\frac{U}{U_0} = (1-\phi)^{4.65}. \tag{5}$$

This expression is widely used in engineering applications even though it is known to deviate from Batchelor's prediction in the limit of small ϕ. The value of the exponent in the RZ expression varies depending on the source, due to variation in the Reynolds and Péclet numbers in different applications, but the form $(1-\phi)^m$ is widely used, where m is typically $O(4\text{-}6)$. For Brownian hard-spheres, a value of $m = 5.40$ is often used. The correct low-ϕ behavior can be obtained without losing accuracy at large ϕ by modifying the Richardson-Zaki expression to force agreement with Batchelor in the dilute limit [7],

$$\frac{U}{U_0} = \frac{(1-\phi)^m}{1+(6.55-m)\phi}. \tag{6}$$

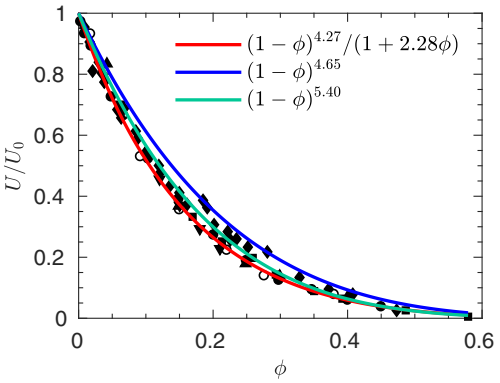

FIG. 5. Settling rates for colloidal hard spheres. The lines represent different expressions of a Richardson-Zaki-like form including (6) with $m = 4.27$. This particular expression fits the settling rates at high concentrations at least as well as the other expressions, but does a better job accounting for variations in the settling rate at low concentrations. The data points are drawn from the literature: squares [29], triangles [30], upside-down triangles [31], diamonds [32], solid circles [33], and open circles [34].

The value of m could be determined by fitting Eq. (6) to the hard-sphere data from our simulations. With this procedure, the value is found to be 3.77. Cichocki *et al.* computed the ϕ^2 contribution to U/U_0 from the three-particle contribution, determining that $U/U_0 = 1 - 6.55\,\phi + 21.92\,\phi^2$ [28]. Using this result, m can be determined by matching the ϕ^2 term in Eq. (6) to the result of Cichocki *et al.* to get $m = 4.27$. In this way, the model parameters are fully specified by known analytical results and no data fitting is required. Equation (6) with the $m = 4.27$ is plotted as the solid black line in Fig. 6(d), and the relative error with respect to the simulated data is smaller than 0.1% for all the volume fractions studied. The inferred and best-fit power-law exponents are less than the values commonly used in the Richardson-Zaki correlation, but Fig. 5 shows that our model quantitatively describes hard-sphere colloidal sedimentation data at least as well as the two other Richardson-Zaki-like correlations used in the literature: $U/U_0 = (1-\phi)^{4.65}$ and $U/U_0 = (1-\phi)^{5.40}$. However, (6) has the added bonus of recovering the dilute-limit predictions of Batchelor precisely.

Inspired by this approach, we notice that further modifying (5) with a denominator $1 + (6.55 - m)\phi - 0.89\phi/\tau$ would also recover Batchelor's predictions in the dilute limit for attractive dispersions. Because the settling rate bears such qualitative similarity with hard spheres at high concentrations, we proceed with the ansatz that the net effect of interparticle attractions can then be accounted for by simply replacing Batchelor's $-0.89\phi/\tau$ with a more general term $-0.89\,f(\phi,\tau)$. This function, $f(\phi,\tau)$, must be bounded from above to avoid singularities. It also must scale as ϕ/τ in the dilute limit and must approach zero in the hard-sphere limit. In principle, this function serves to interpolate between hard-sphere settling rate and the settling rate of aggregated dispersions. The empirical expression we propose for the settling rate is

$$\frac{U}{U_0} = \frac{(1-\phi)^{4.27}}{1 + 2.28\,\phi - 0.89\,f(\phi,\tau)}, \tag{7}$$

where a form for $f(\phi,\tau)$ remains to be specified.

This hypothesized model can be tested by solving (7) for $f(\phi,\tau)$, and computing this quantity from known settling rates. Figure 6 shows the values of $f(\phi,\tau)$, as a function of ϕ/τ with the settling rates given by our simulation data and the experimental data of Lattuada *et al.* All the data in Fig. 6 falls along a single master curve. For small values of ϕ/τ, $f(\phi,\tau)$ is linear in ϕ/τ with a slope of 1. This is required in order to recover Batchelor's predictions in the dilute limit. At large ϕ/τ, the $f(\phi,\tau)$ saturates. Note the maximal value of ϕ/τ explored in this work is about 4 ($\phi = 0.4$, $\tau \approx 0.1$). For $\tau < 0.1$, adhesive hard spheres phase separate, and we have sought to stay within

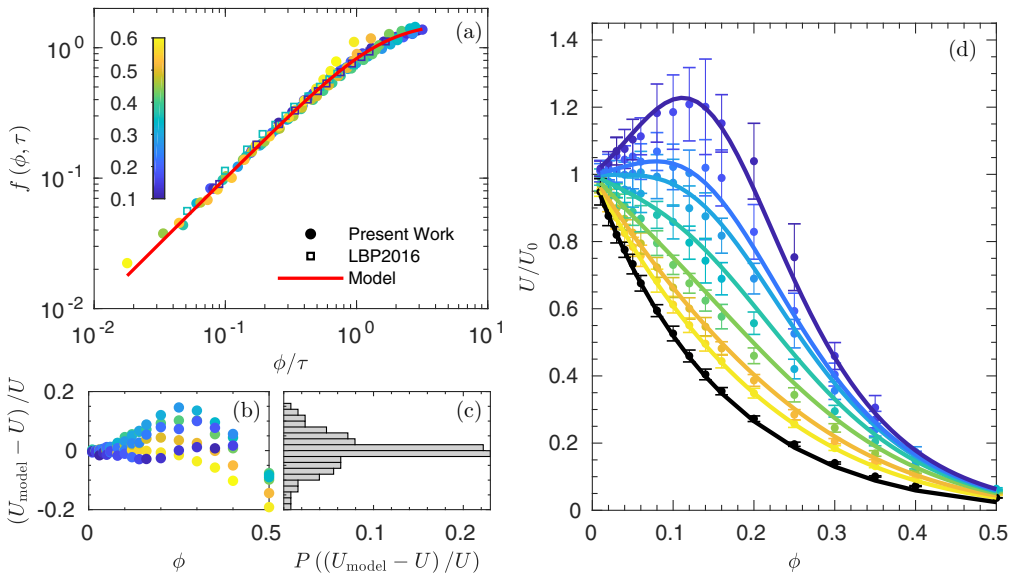

FIG. 6. (a) Interparticle interaction contribution to the hindered and promoted settling functions given in Eq. (7) with $m = 4.27$ as a function of the normalized volume fraction for a range of τ computed from sedimentation data in the present work (circles) and the experimental data of Ref. [9] (open squares, denoted LBP2016 in the legend). Hard-sphere data, for which $f = 0$, has been omitted. The red line is given by Eq. (8). The color of each data point corresponds to the τ value determined by fitting $S(q)$ to the AHS model. (b) Relative error in the computed model velocity U_{model} given by Eq. (7) compared to the observed velocity U as a function of volume fraction. (c) Observed probability distribution for the relative error in the model prediction. (d) Settling rates predicted by the model (7) for $\tau = [0.106, 0.125, 0.136, 0.165, 0.219, 0.322, 0.484, \infty]$ (lines) compared to the simulation results (Fig. 4), with the same coloring as in panel (a). Hard-sphere data, for which $\tau = \infty$, is shown in black.

the single-phase region for all the present calculations. The function $f(\phi,\tau)$ can be described by a sigmoidal function of ϕ/τ. There are many possible choices for this function, but a compact and convenient one is

$$f(\phi,\tau) = \frac{\phi/\tau}{[1 + n\,(\phi/\tau)^p]^{1/p}}, \tag{8}$$

where p is a fitting parameter that is varied along with n to minimize the sum of squared errors between the model prediction for U and the data. The optimal values computed by a nonlinear least squares fit to the entire data set are $n = 0.43$ and $p = 1.85$.

The model accurately describes the settling rate across the wide range of ϕ and τ studied. The relative error of the model with respect to the data is plotted in Fig. 6(b). The relative error is smaller than 20% for all the cases studied. The model does tend to slightly overpredict the settling rate at modest τ and is the least accurate for the stronger attractions studied. This can be understood by recognizing that for the strongly attractive particles, $\tau \approx 0.1$, which is very close to the theoretical critical Baxter temperature, $\tau = 0.098$. For modest τ, the physical picture is that particles aggregate into transient clusters, which distribute homogeneously in the dispersion. However, in the neighborhood of the boundary for liquid-liquid phase separation, the system exhibits large particle number density fluctuations. This produces large fluctuations in the mean settling rate that are quantified by the standard error in Fig. 4. In spite of this physical limitation, the results of the empirical model appear to provide good predictions of the settling rate even in this region of phase space.

D. Inferring macromolecular interactions through application of the settling model

One potential application of the proposed model is for inference of the interactions between suspended colloids through mapping onto the AHS model. An important use case is the characterization of attractive interactions between macromolecular species such as proteins in concentrated solutions and under varying solution conditions. Such characterization is needed for the purification, dewatering, and storage of biologics in pharmaceutical applications. Utilizing a hydrodynamic and thermodynamic model for rigid spherical colloids to describe macromolecules which are neither spherical nor rigid has a long tradition in macromolecular sciences stemming primarily from application of the Stokes-Einstein relation to estimate the hydrodynamic radius. In the context of proteins, transport properties in these solutions are commonly investigated using dynamic light scattering. In light scattering experiments, the correlation of the scattering intensity with time, t, is used to compute the so-called intermediate scattering function, $F(q,t)$, which depends on a scattering wave vector q. For short correlation times, the value of this function is a direct measurement of the static structure factor, $S(q) = F(q,0)$, and its rate of change can be used to compute a wave-vector-dependent diffusivity, $D(q) = -q^{-2}(d/dt)\log[F(q,t)/F(q,0)]$ as $t \to 0$. As $q \to 0$, $D(q)$ is just the collective diffusivity D_C and is related to the sedimentation coefficient, U/U_0, of the macromolecule by the simple relation

$$D_C = \frac{D_0}{S(0)}\frac{U}{U_0}. \tag{9}$$

Here, D_0 is the diffusion coefficient of the macromolecule at infinite dilution. Therefore, dynamic light scattering measurements for small scattering wave vectors can be used to simultaneously measure the collective diffusivity and $S(0)$, which is linearly proportional to the isothermal compressibility of the macromolecular component of the solution.

For dilute solutions of macromolecules, measurements of these two quantities is part of the standard suite of macromolecular characterizations. In the dilute limit, $S(0) = 1 + k_S vc$ and $D_C = D_0(1 + (k_S - k_H)vc)$. Here, c is the molar concentration of macromolecules in solution and v is the molar volume of the macromolecule. The dimensionless coefficient k_S is purely thermodynamic in origin and linearly proportional to the second virial coefficient. The dimensionless coefficient k_H describes the linear variations in the sedimentation coefficient of the macromolecular solution. For the sticky sphere dispersions described in the previous sections, $v = 4\pi a^3 N_A/3$, with N_A Avogadro's number, $k_S = -8 + 2/\tau$, $k_H = 6.55 - 0.89/\tau$. From the slope of D_C and $S(0)$, the quantities vk_S and vk_H can be computed. If the sticky sphere model is deemed applicable, then the molar volume and the stickiness parameter are computed instead. The advantage of this latter approach is that v and τ can be used to locate the macromolecular solution on the AHS phase diagram.

Beyond the dilute limit, more sophisticated models are needed. The AHS model for $S(0)$ is known analytically from the Percus-Yevick closure approximation applied to the Ornstein-Zernicke equation for the direct correlation function:

$$S(0) = \left[\frac{(1-\phi)^2}{1 + 2\phi - \lambda(\phi,\tau)\,\phi\,(1-\phi)}\right]^2, \tag{10}$$

where

$$\lambda(\phi,\tau) = 6\left(\frac{\tau}{\phi} + \frac{1}{1-\phi}\right) - \left[36\left(\frac{\tau}{\phi} + \frac{1}{1-\phi}\right)^2 - 12\frac{1+0.5\phi}{\phi\,(1-\phi)^2}\right]^{1/2}. \tag{11}$$

From the present work, Eq. (7) models the sedimentation coefficient, $U/U_0 = D_C S(0)/D_0$. To relate experimental data to the two models, the colloidal volume fraction must be defined in terms of the molar concentration c as $\phi = vc$. Then, the experimental system has the properties of the sticky sphere solution at concentration c and parameterized by a molar volume v and stickiness

parameter τ, just as in the dilute limit. We envision three different modes of inference with these models:

(1) Repeated measurements of $S(0)$ and D_C at a particular concentration, c, and in a particular solution condition (temperature, ionic strength, pH), denoted $\mathbf{p}$, are used to determine the values of $\tau(c,\mathbf{p})$ and $v(c,\mathbf{p})$ for a corresponding AHS dispersion.

(2) Measurements of $S(0)$ and D_C are made at different macromolecular concentrations and a particular solution condition, and a nonlinear least squares fit assuming a constant molar volume but concentration-dependent stickiness parameter is used to find the set of parameters: $v(\mathbf{p})$, $\tau(c,\mathbf{p})$.

(3) $S(0)$ and D_C are measured as function of the solution conditions at a particular macromolecule concentrations, and a nonlinear least squares fit of the data to the model is used to determine the parameters, $v(\mathbf{p})$ and $\tau(\mathbf{p})$, descriptive of the data across the entire range of concentrations.

Choice of inference scheme depends on the particular macromolecule under study; one could proceed from one scheme to the next should the assumptions of concentration-independent molar volume and stickiness prove sound.

Muschol and Rosenberger used light scattering experiments to measure $S(0)$ and D_C of concentrated lysozyme solutions at high ionic strengths for which long-range electrostatic repulsions are screened and the macromolecules behave much like sticky spheres [36]. Because we neither designed nor performed the experiments, we choose the third inference problem which determines the molar volume and stickiness parameter as a function of the solution conditions alone. Lysozyme is a globular protein with an ellipsoidal shape having major and minor semiaxes of $a = 2.75$ nm and $b = c = 1.65$ nm, and typical molecular weight of 14 kDa [37]. Based on the dimensions of the effective ellipsoid, a molar volume associated with the molecule $v = 4\pi abcN_A/3 = 18.9\,\mathrm{M}^{-1}$ is anticipated. The lysozyme is suspended in a sodium acetate buffer whose concentration is varied between 50 and 1470 mM. Additionally, for a 50-mM NaAc buffer, NaCl is added to the solution at concentrations up to 472 mM. For each solution condition, $S(0)^{-1}$ and U/U_0 were reported for lysozyme concentrations up to 70 mg/mL. On the basis of the estimated molar volume, the maximum concentration is equivalent to a volume fraction of approximately 10%.

Figure 7 depicts these measurements as well as fits of the AHS model under each solution condition. The models do a remarkable job of capturing the experimental data across a range of volume fractions. In particular, Eq. (7) appears to describe the settling behavior of the proteins very well in conditions for which the dilute limit expressions of Batchelor would fail. Table I reports the

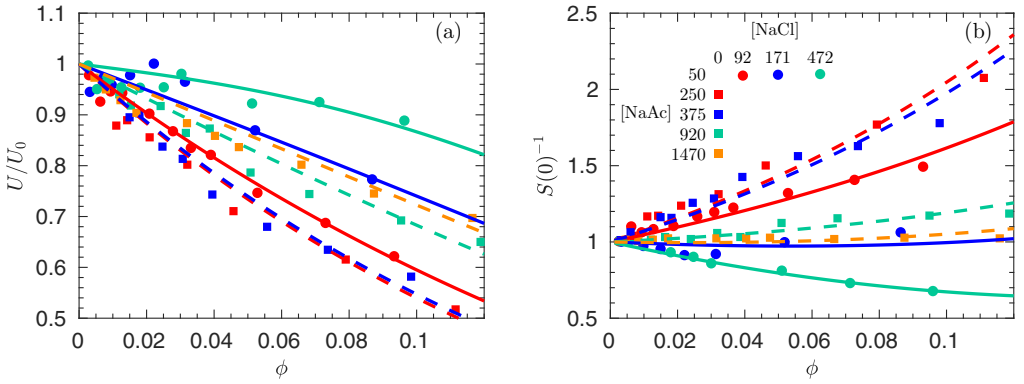

FIG. 7. Sedimentation coefficient (a) and static structure factor (b) measured in Ref. [35] for concentrated solutions of lysozyme. Circles correspond to fixed buffer strength and varying added salt. Add concentrations are reported in units of mM. Squares correspond to no added salt but varying buffer strength. The solid and dashed lines are the best fits of the AHS models to the data for circles and squares, respectively. The experimental data is presented as in Ref. [35], but with the concentration, c, recast as the volume fraction on multiplication by the inferred molar volume.

TABLE I. Stickiness parameter and molar volume inferred from nonlinear least squares fit of AHS model to experimental measurements of $S(0)$ and U/U_0 in lysozyme solutions [35].

	τ	v
[NaCl]	[NaAc] = 50 mM	
92 mM	0.59	19.8 M^{-1}
171 mM	0.22	23.6 M^{-1}
472 mM	0.16	21.3 M^{-1}
[NaAc]	[NaCl] = 0 mM	
250 mM	2.7	22.3 M^{-1}
375 mM	1.8	20.1 M^{-1}
920 mM	0.29	23.7 M^{-1}
1470 mM	0.24	24.4 M^{-1}

molar volume and the stickiness parameters inferred from fits to the experimental data. For 50-mM buffer, the molar volume averages 21.6 M^{-1}, while the stickiness parameter decreases with added salt. Increasing the ionic strength of the solution decreases the Debye layer thickness associated with electrostatic repulsions that stabilize the proteins against aggregation. On decreasing the Debye layer thickness, the macromolecular solutions appear more sticky. With no added salt, but higher buffer concentration, the molar volume of the lysozyme is larger and averages 22.6 M^{-1}. With increasing added buffer, the proteins also appear to grow stickier.

The two lysozyme solutions with [NaCl] = 92 mM and [NaAc] = 250 mM have ionic strengths that differ by less that 5%. The same is true of the ([NaCl], [NaAc]) pairs (171, 375) mM and (472, 920) mM. Consequently, the electrostatic interactions between the proteins are similar screened in each of these cases. However, the stickiness parameters and molar volumes inferred from the AHS hard-sphere models show no correspondence. This same lack of correspondence is evident in the $S(0)$ and U/U_0 data itself. It is known that there are specific ion effects in concentrated electrolyte solutions that sensitively affect the interactions between charged colloids such as proteins [38]. These specific effects alter the structure factor and transport properties of the lysozyme solutions in ways that are difficult to predict with classical Dejaguin-Landau-Verwey-Overbeek (DLVO) theory [39]. However, inference of the molar volume and stickiness parameter from fitting the AHS model to DLS data is sufficient to characterize solution in a way that yields an accurate description of thermodynamic properties (isothermal compressibility) and transport properties (sedimentation coefficient).

IV. CONCLUSION

We present coarse-grained simulations of the sedimentation of sticky particle suspensions that are shown to be in quantitative agreement with published experimental data. We systematically studied the effect of interparticle attraction strength and volume fraction on the mean sedimentation rate of the suspensions, observing a smooth transition with increasing attraction strength from hard-sphere sedimentation to nonmonotonic promoted settling due to particle aggregation. We developed a simple model for the sedimentation rate by modifying a Richardson-Zaki-like expression to match Batchelor's dilute limit prediction and including a function that extrapolates between hard-sphere-like and aggregated states. The model quantitatively describes the simulation data up to the percolation phase boundary, and an example application of this model to the study of collective protein diffusion is illustrated. The mapping of sticky particle suspensions onto an effective AHS model is generic and can be used to infer sedimentation and diffusion behavior across a range concentrations from light scattering measurements made at only a few concentrations, even in suspensions where the particles are not uniform or spherical, provided the attractions are sufficiently short-ranged and the particle aspect ratio is not too large.

ACKNOWLEDGMENTS

J. Swan and A. Fiore gratefully acknowledge funding from the MIT Energy Initiative Shell Seed Fund and NSF Career Award No. CBET-1554398. The authors also thank Roberto Piazza for suggesting the model exponent be determined by matching the result of Cichocki *et al.*

[1] J. Lebowitz, M. S. Lewis, and P. Schuck, Modern analytical ultracentrifugation in protein science: A tutorial review, Protein Sci. **11**, 2067 (2002).
[2] D. Lerche, Dispersion stability and particle characterization by sedimentation kinetics in a centrifugal field, J. Dispersion Sci. Technol. **23**, 699 (2002).
[3] W. H. Rulkens, R. Tichy, and J. T. C. Grotenhuis, Remediation of polluted soil and sediment: Perspectives and failures, Water Sci. Technol. **37**, 27 (1998).
[4] E. Partheniades, Erosion and deposition of cohesive soils, J. Hydraulics Div. **91**, 105 (1965).
[5] R. Roa, E. K. Zholkovskiy, and G. Nägele, Ultrafiltration modeling of non-ionic microgels, Soft Matter **11**, 4106 (2015).
[6] E. Guazzelli and J. Hinch, Fluctuations and instability in sedimentation, Annu. Rev. Fluid Mech. **43**, 97 (2011).
[7] G. K. Batchelor, Sedimentation in a dilute dispersion of spheres, J. Fluid Mech. **52**, 245 (1972).
[8] G. K. Batchelor, Sedimentation in a dilute polydisperse system of interacting spheres. Part 1. General theory, J. Fluid Mech. **119**, 379 (1982).
[9] E. Lattuada, S. Buzzaccaro, and R. Piazza, Colloidal Swarms Can Settle Faster than Isolated Particles: Enhanced Sedimentation Near Phase Separation, Phys. Rev. Lett. **116**, 038301 (2016).
[10] J. W. Swan and G. Wang, Rapid calculation of hydrodynamic and transport properties in concentrated solutions of colloidal particles and macromolecules, Phys. Fluids **28**, 011902 (2016).
[11] F. B. Usabiaga, B. Kallemov, B. Delmotte, A. P. S. Bhalla, B. E. Griffith, and A. Donev, Hydrodynamics of suspensions of passive and active rigid particles: A rigid multiblob approach, Commun. Appl. Math. Comput. Sci. **11**, 217 (2016).
[12] A. M. Fiore, F. Balboa Usabiaga, A. Donev, and J. W. Swan, Rapid sampling of stochastic displacements in Brownian dynamics simulations, J. Chem. Phys. **146**, 124116 (2017).
[13] A. M. Fiore and J. W. Swan, Rapid sampling of stochastic displacements in Brownian dynamics simulations with stresslet constraints, J. Chem. Phys. **148**, 044114 (2018).
[14] J. Rotne and S. Prager, Variational treatment of hydrodynamic interaction in polymers, J. Chem. Phys. **50**, 4831 (1969).
[15] D. Lindbo and A.-K. Tornberg, Spectrally accurate fast summation for periodic Stokes potentials, J. Comput. Phys. **229**, 8994 (2010).
[16] C. Keller, N. I. M. Gould, and A. J. Wathen, Constraint preconditioning for indefinite linear systems, SIAM J. Matrix Anal. Appl. **21**, 1300 (2000).
[17] A. A. Zick and G. M. Homsy, Stokes flow through periodic arrays of spheres, J. Fluid Mech. **115**, 13 (1982).
[18] P. N. Segre, E. Herbolzheimer, and P. M. Chaikin, Long-Range Correlations in Sedimentation, Phys. Rev. Lett. **79**, 2574 (1997).
[19] S. Asakura and F. Oosawa, On interaction between two bodies immersed in a solution of macromolecules, J. Chem. Phys. **22**, 1255 (1954).
[20] A. J. C. Ladd, H. Gang, J. Zhu, and D. A. Weitz, Temporal and spatial dependence of hydrodynamic correlations: Simulation and experiment, Phys. Rev. E **52**, 6550 (1995).
[21] M. G. Noro and D. Frenkel, Extended corresponding-states behavior for particles with variable range attractions, J. Chem. Phys. **113**, 2941 (2000).
[22] A. Moncho-Jordá, A. A. Louis, and J. T. Padding, Effects of Interparticle Attractions on Colloidal Sedimentation, Phys. Rev. Lett. **104**, 068301 (2010).

[23] B. Cichocki and K. Sadlej, Steady-state particle distribution of a dilute sedimenting suspension, EPL **72**, 936 (2005).
[24] R. J. Baxter, Percus–Yevick equation for hard spheres with surface adhesion, J. Chem. Phys. **49**, 2770 (1968).
[25] J. K. Percus and G. J. Yevick, Analysis of classical statistical mechanics by means of collective coordinates, Phys. Rev. **110**, 1 (1958).
[26] C. Regnaut and J. C. Ravey, Erratum: Application of the adhesive sphere model to the structure of colloidal suspensions [J. Chem. Phys. **91**, 1211 (1989)], J. Chem. Phys. **92**, 03250(E) (1990).
[27] J. F. Richardson and W. N. Zaki, The sedimentation of a suspension of uniform spheres under conditions of viscous flow, Chem. Eng. Sci. **3**, 65 (1954).
[28] B. Cichocki, M. L. Ekiel-Jeżewska, P. Szymczak, and E. Wajnryb, Three-particle contribution to sedimentation and collective diffusion in hard-sphere suspensions, J. Chem. Phys. **117**, 1231 (2002).
[29] J.-Z. Xue, E. Herbolzheimer, M. A. Rutgers, W. B. Russel, and P. M. Chaikin, Diffusion, Dispersion, and Settling of Hard Spheres, Phys. Rev. Lett. **69**, 1715 (1992).
[30] J.-C. Bacri, C. Frenois, M. Hoyos, R. Perzynski, N. Rakotomalala, and D. Salin, Acoustic study of suspension sedimentation, EPL **2**, 123 (1986).
[31] S. Buzzaccaro, A. Tripodi, R. Rusconi, D. Vigolo, and R. Piazza, Kinetics of sedimentation in colloidal suspensions, J. Phys.: Condens. Matter **20**, 494219 (2008).
[32] C. G. de Kruif, J. W. Jansen, and A. Vrij, Sterically stabilized silica colloid as a model supramolecular fluid, in *Physics of Complex and Supramolecular Fluids*, edited by S. A. Safran and N. A. Clark (John Wiley & Sons, New York, 1987), p. 315.
[33] R. Buscall, J. W. Goodwin, R. H. Ottewill, and T. F. Tadros, The settling of particles through Newtonian and non-Newtonian media, J. Colloid Interface Sci. **85**, 78 (1982).
[34] A. J. C. Ladd, Hydrodynamic transport coefficients of random dispersions of hard spheres, J. Chem. Phys. **93**, 3484 (1990).
[35] M. Muschol and F. Rosenberger, Interactions in undersaturated and supersaturated lysozyme solutions: Static and dynamic light scattering results, J. Chem. Phys. **103**, 10424 (1995).
[36] R. Piazza, V. Peyre, and V. Degiorgio, "Sticky hard spheres" model of proteins near crystallization: A test based on the osmotic compressibility of lysozyme solutions, Phys. Rev. E **58**, R2733 (1998).
[37] S. B. Dubin, N. A. Clark, and G. B. Benedek, Measurement of the rotational diffusion coefficient of lysozyme by depolarized light scattering: Configuration of lysozyme in solution, J. Chem. Phys. **54**, 5158 (1971).
[38] M. Z. Bazant, B. D. Storey, and A. A. Kornyshev, Double Layer in Ionic Liquids: Overscreening Versus Crowding, Phys. Rev. Lett. **106**, 046102 (2011).
[39] M. Boström, D. R. M. Williams, and B. W. Ninham, Specific Ion Effects: Why DLVO Theory Fails for Biology and Colloid Systems, Phys. Rev. Lett. **87**, 168103 (2001).